

PHYSICAL REVIEW B

CONDENSED MATTER

THIRD SERIES, VOLUME 39, NUMBER 16 PART A

1 JUNE 1989

Mössbauer spectrometry study of the hyperfine fields and electronic structure of Fe-Co alloys

H. H. Hamdeh, B. Fultz, and D. H. Pearson

Division of Engineering and Applied Science 138-78, California Institute of Technology, Pasadena, California 91125

(Received 14 October 1988; revised manuscript received 31 January 1989)

We obtained ^{57}Fe hyperfine-field parameters from Mössbauer spectra of Fe-Co alloys at 77 and 295 K. We also obtained the numbers of $3d$ electrons at Fe atoms by electron-energy-loss spectrometry (EELS). Together with bulk-magnetization data, we deduce how the occupancies of the $3d\uparrow$ and $3d\downarrow$ states at Fe atoms change with Co concentration. Changes in the total numbers of $3d$ electrons at Fe atoms were found to be small, with the Mössbauer data indicating a maximum of about 0.2 electrons at 30 at. % Co, and the EELS data indicating a change of similar magnitude but of opposite sign. From both our isomer-shift and hyperfine-magnetic-field (HMF) data, we deduce a slight reduction in the occupancy of $4s$ states with Co concentration of $dn_{4s}/dc = -0.02$ electrons, which is principally due to a loss of $4s\downarrow$ electrons. The model employed for the calculation of HMF distributions in terms of conduction- and core-electron polarizations worked well for disordered Fe-Co alloys, and was used to analyze the changes in HMF after the disorder \rightarrow order transformation. It showed that these HMF changes upon ordering are primarily due to changes in conduction-electron polarization.

I. INTRODUCTION

Much effort, both experimental and theoretical, has been devoted to studies of the interesting ferromagnetic properties of bcc Fe-Co alloys. The Slater-Pauling curve of bulk magnetization versus Co concentration rises to a rather sharp peak at about 30 at. % Co, and then decreases with further Co concentration. Iron and Fe-rich alloys are weak ferromagnets with the Fermi level intersecting both the $3d\uparrow$ and $3d\downarrow$ spin bands, while Co is a strong ferromagnet, having holes only in its $3d\downarrow$ band. With this transition from weak to strong ferromagnetism, the basic shape of the Slater-Pauling curve and the occupancy of the $3d\uparrow$ states can be understood,¹⁻⁴ but there remain questions about how the occupancies of the $3d\downarrow$ states and the s -like states depend on Co concentration.

Mössbauer spectrometry complements experimental data on bulk magnetic properties. The hyperfine-magnetic-field (HMF) at the ^{57}Fe nucleus, H , originates mainly from the Fermi contact interaction, and is proportional to the imbalance in spin density of the s -like electrons at the ^{57}Fe nucleus. The spin polarization of these electrons of s symmetry is caused by their exchange interactions with the unpaired $3d$ electrons local to the ^{57}Fe atom, as well as by exchange interactions with $3d$ electrons at neighboring atoms. Consequently the HMF is sensitive to the magnetic moment at the ^{57}Fe atom, as well as to magnetic moments at atoms in its local envi-

ronment. The isomer shift I which is proportional to the total density of s electrons at the ^{57}Fe nucleus, is another important contact interaction that also depends on the electronic structure of the ^{57}Fe atom and its environment.

Previous Mössbauer spectrometry investigations of concentrated Fe-Co alloys⁵⁻¹⁰ did not provide complete interpretations of the measured HMF's and isomer shifts. These studies were performed at room temperature, and interpretations of such data are impaired by spin-wave excitations. Furthermore, many such studies^{7,9,10} analyzed the ^{57}Fe HMF distribution in terms of a model, originally due to Wertheim, *et al.*,¹¹ which assumes an additivity of the ^{57}Fe HMF perturbations from solutes in the first few nearest-neighbor shells of ^{57}Fe nuclei. Although this model successfully describes the effects of many solutes in Fe metal, we show that it is inappropriate for nondilute Fe-Co alloys. Other workers analyzed the ^{57}Fe HMF distribution in terms of systematic changes in conduction electron and core polarizations,^{5,6} and showed that the mean ^{57}Fe HMF in nondilute Fe-Co alloys can be understood in this way. These systematics were further developed by Stearns,^{12,13} who interpreted a cryogenic NMR study of dilute Fe-Co alloys by Budnick, *et al.*¹⁴ in a manner similar to that used in the present work.

By using the normalized intensities of the "white lines" at L_2 and L_3 absorption edges, it was recently demonstrated that it is possible to determine a local density of

3d electrons about transition metal atoms by electron-energy-loss spectrometry (EELS) in a transmission electron microscope.¹⁵ These white lines originate from excitations of 2p electrons to unoccupied 3d states, so the intensity of the white lines is proportional to the number of 3d holes at the transition metal atom. In the present work we use the white-line correlation from this previous work as an additional means to determine changes in the number of 3d electrons about Fe atoms in different Fe-Co alloys.

Some experimental details of the Mössbauer spectrometry and the electron-energy-loss-spectrometry measurements are provided in Sec. II. By combining the isomer shift and bulk magnetization data in Sec. III, we find the average electronic configuration for Fe atoms in Fe-Co alloys. We evaluate the relationship between the change in isomer shift and the change in number of 3d electrons, dI/dn_{3d} , and we report evidence for a change in population of 4s states with Co concentration. In Sec. IV we describe the analysis of the ⁵⁷Fe HMF distribution in terms of core polarization and conduction-electron polarization. In Sec. V we combine the HMF data with the magnetic-moment data to calculate the dependence of HMF on Co concentration. A lack of agreement is attributed to a reduction in occupancy of 4s↓ states, which is consistent with the reduction in 4s population with Co concentration obtained in Sec. III. Changes in the ⁵⁷Fe HMF distribution and isomer shift as a result of B2 chemical ordering in Fe-Co are discussed in Sec. VI.

II. EXPERIMENT AND DATA ANALYSIS

Samples of Fe_{1-c}Co_c were prepared from materials of 99.99% purity. Alloys with Co concentrations of 4.62% (all compositions are in atomic percent), 9.44%, 20%, 31%, and 50% were arc melted, while alloys with Co concentration of 40%, 60%, and 70% were induction melted. All melting was performed under argon atmospheres, and all ingots were inverted and remelted several times to ensure homogeneity. Mass losses after melting were negligible, hence the alloys' compositions were obtained from the masses of the starting materials. The chemical compositions of some alloys were also measured by atomic absorption and x-ray fluorescence spectrometries. X-ray diffractometry employing a G.E. XRD-5 θ -2 θ diffractometer with Cr K α radiation was performed on representative specimens of material before and after heat treatments. The materials were found to be entirely bcc polycrystals; occasionally B2 superlattice peaks were barely visible. Similar results were obtained by transmission-electron-microscopy examination.

The alloys were subjected to two different heat treatments. In the first heat treatment, intended to produce chemically disordered alloys, filings were melted and subjected to piston-anvil quenching, which has a characteristic cooling rate of 10⁵–10⁶ °C/sec. In the second heat treatment, intended to produce ordered alloys, filings were heated at 800 °C inside evacuated quartz ampules for several hours, and then gradually cooled to ~300 °C during two days before being cooled to room tempera-

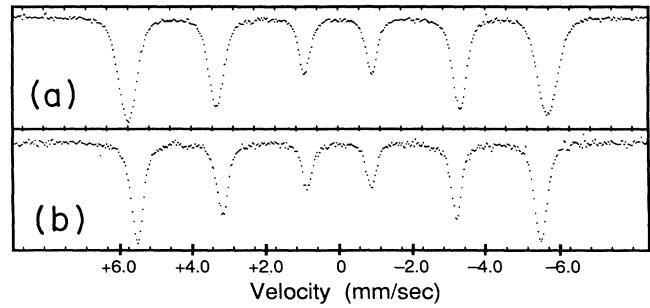


FIG. 1. Mössbauer spectra obtained at 77 K of Fe-50 at. % Co samples that were (a) pistonanvil quenched (disordered), and (b) annealed at progressively lower temperatures (ordered).

ture. Electron-transparent foils were chemically thinned from some of the materials. These specimens were analyzed with a Gatan 607 electron energy loss spectrometer on a Philips EM 430 transmission electron microscope. The microscope was operated at 200 kV in diffraction mode, using a camera length of 80 mm and a spectrometer collection aperture of 3 mm. Spectra were obtained from several regions of each specimen.

Mössbauer spectra were obtained in transmission geometry with a conventional constant-acceleration spectrometer. Spectra were obtained both at 295 K and at 77 K. A radiation source of 30 mCi ⁵⁷Co in a Rh matrix was used for all measurements. The spectrometer velocity calibration was checked after every few runs by obtaining spectra from a pure Fe foil. The specimens used in this work were about 15- μ m thick, and no thickness-distortion corrections were employed. Thickness-distortion corrections will modify our results for the variance of the HMF distribution of the Fe-rich specimens. Examples of Mössbauer spectra taken at 77 K from ordered and disordered alloys of Fe-50 at. % Co are presented in Fig. 1. Notice the reduction of the mean and variance of the HMF distribution upon ordering.

In disordered Fe-Co alloys, the HMF distribution results in a broadening and outward shift of all the lines of the Mössbauer spectra with respect to those of pure Fe. Hyperfine-magnetic-field and isomer-shift data were obtained from the measured spectra by three methods. In the first, a skewed Gaussian distribution was used:

$$P(H) = A [1 - \kappa(H - H_0)] \exp \left[- \left(\frac{H - H_0}{\sigma} \right)^2 \right], \quad (1)$$

where A is a normalization constant, σ is related to the width, and κ is a skewness parameter. This HMF distribution was convolved with a sextet of Lorentzian lines characteristic of a pure Fe spectrum, and a least-squares fit to the experimental data was performed. In addition to the mean position of the spectrum (which provided the average isomer shift), the parameters A , σ , and κ were all freely adjusted in the fitting routine. In the second method, the Mössbauer spectra were fit to a single sextet of Lorentzian lines. This method is good enough to provide the mean HMF and mean isomer shift, and these

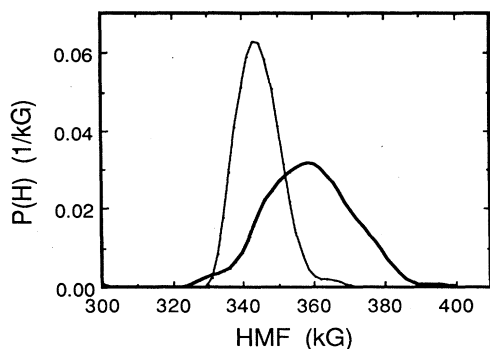


FIG. 2. Hyperfine-magnetic-field distributions obtained from the data of Fig. 1 by the method of Le Cäer and Dubois. Dark curve: disordered alloy. Light curve: ordered alloy.

data were in full agreement with those of the first method within the statistical error of the data. The third method employed the HMF analysis procedure of Le Cäer and Dubois,¹⁶ and assumed a continuous distribution of HMF's. This method gave results for the mean and variance of the HMF distribution that were essentially identical to those of the first method. The HMF distributions obtained from the data of Fig. 1 by the method of Le Cäer and Dubois are presented in Fig. 2.

III. ISOMER SHIFTS, ELECTRON-ENERGY-LOSS SPECTRA, AND MAGNETIZATION DATA

Bulk magnetizations of Fe-Co alloys have been measured by Bardos.¹⁷ His data, and those of earlier work,¹⁸ show that the mean magnetic moment increases with Co concentration to a maximum at around 30 at. % Co, and then decreases. Theoretical^{4,19,20} and neutron-diffraction²¹ studies show that the increase in the mean magnetic moment is due to an increase in magnetic moment at Fe atoms; the Co magnetic moment stays approximately constant. By taking the Co magnetic moment to be $1.85\mu_B$,¹² we obtained the variation of Fe magnetic moment with Co concentration that is presented in Fig. 3. The Fe magnetic moment increases from $2.22\mu_B$ for pure Fe to about $3.0\mu_B$ at 70 at. % Co.

The Fe magnetic moment is carried by its $3d$ electrons, whose total number was determined by electron energy loss spectrometry. Using the calibration of the white-line intensity versus number of $3d$ electrons that was obtained previously,¹⁵ we obtained data for the number of $3d$ electrons at Fe atoms in different Fe-Co alloys that are presented in Fig. 4. These EELS measurements showed a change in the total number of $3d$ electrons at Fe atoms (about -0.3 ± 0.1 electron) that is much smaller than the increase in Fe magnetic moment ($+0.73$ electron at 70 at. % Co). Clearly a simple transfer of electrons either into Fe $3d \uparrow$ states or out of Fe $3d \downarrow$ states is not how the Fe magnetic moment changes during alloying; both changes must occur together.

To interpret the Mössbauer isomer shift in conjunction with the magnetization data for disordered alloys, we assumed that the $3d \uparrow$ states are gradually filled to capacity

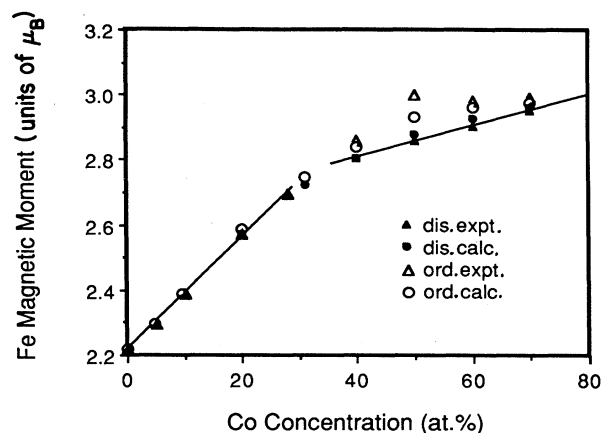


FIG. 3. The mean-magnetic moment of Fe atoms in Fe-Co alloys, μ_{Fe} , vs Co concentration of disordered (dis.) and ordered (ord.) alloys, assuming $\mu_{Co} = 1.85\mu_B$. The solid lines are least-squares fit to the experimental data of the disordered phase. The calculated curves were obtained from the simulations described in Sec. IV.

at about 30 at. % Co, while the $3d \downarrow$ states are continuously emptied with increasing Co concentration.^{1-4,19,22} We fit the Fe moment data of Fig. 3 for the disordered phase to a straight line for Co concentrations less than 30 at. %, and as a straight line of lesser slope for Co concentrations greater than 30 at. %. For Co concentrations greater than 30 at. % we assume that $dn_{3d \uparrow}/dc = 0$, so in this regime we obtain the loss of electrons from Fe $3d \downarrow$ states: $dn_{3d \downarrow}/dc = -0.48$. Extrapolating this emptying of Fe $3d \downarrow$ states to the lower Co concentrations, to fit the first straight line of Fig. 3 we must have an increase in the Fe $3d \uparrow$ states: $dn_{3d \uparrow}/dc = +1.20$. The total occupancy of Fe $3d$ states at these low Co concentrations changes with Co concentration as $dn_{3d}/dc = +0.72$, while above 30 at. % Co it is $dn_{3d}/dc = -0.48$. The net change in occupancy of Fe $3d$ states in Fe-50 at. % Co alloys with respect to pure Fe is thus $+0.12$ electron. These small

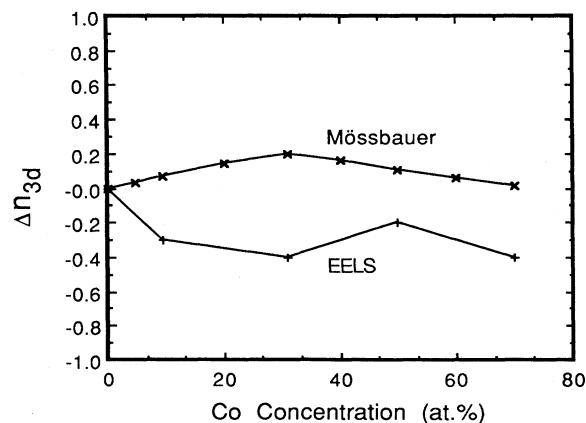


FIG. 4. The number of $3d$ electrons about Fe atoms vs Co concentration, determined with EELS measurements of $L_{2,3}$ white line intensities, and Mössbauer results of Fig. 6.

changes seem consistent with those reported by Szuszkiewicz²³ for the total number of 3d electrons in the alloy.

The variation with Co concentration of isomer shift at 77 K is presented in Fig. 5. These data are similar to our data at 295 K, which are in good agreement with those of Vincze, Campbell, and Meyer.⁵ Although the 4s electrons are delocalized, the 1s, 2s, and 3s electrons at a ⁵⁷Fe atom are too localized to be sensitive to the surrounding Co atoms, except indirectly through their interactions with the 3d electrons at the ⁵⁷Fe atom. The isomer shift will therefore have the following dependence on Co concentration:

$$\frac{dI}{dc} = \frac{\partial I}{\partial n_{3d}} \frac{dn_{3d}}{dc} + \frac{\partial I}{\partial n_{4s}} \frac{dn_{4s}}{dc} \quad (2)$$

As shown in Fig. 5, the isomer shift for disordered alloys has an approximately linear dependence on Co concentration up to 30 at. % Co with $dI/dc = +0.185$, and an approximately linear dependence on Co concentration beyond 30 at. % Co of $dI/dc = -0.055$. The relationship in Eq. (2) therefore gives us two equations (one for each regime of Co concentration), and with $\partial I/\partial n_{4s} = -2.0$ (mm/sec)/electron, as estimated by Walker *et al.*,²⁴ we obtain the two unknowns: $\partial I/\partial n_{3d} \approx +0.2$ (mm/sec)/electron, and $dn_{4s}/dc \approx -0.02$ electrons. The 4s component of the isomer shift is shown independently in Fig. 5, and was subtracted from the measured isomer shift to provide the 3d component of isomer shift, also shown in Fig. 5. We note that by using band theory calculations, Fateseas²⁵ made a diagram of isomer shift versus electronic configuration that is consistent with our value for $\partial I/\partial n_{3d}$. Our result for dn_{4s}/dc is small, but it should be reliable since the isomer shift is much more sensitive to changes in 4s electrons than to changes in 3d electrons. The data of Szuszkiewicz²² on changes in the number of 4s electrons as a function of Co concentration are inconsistent with

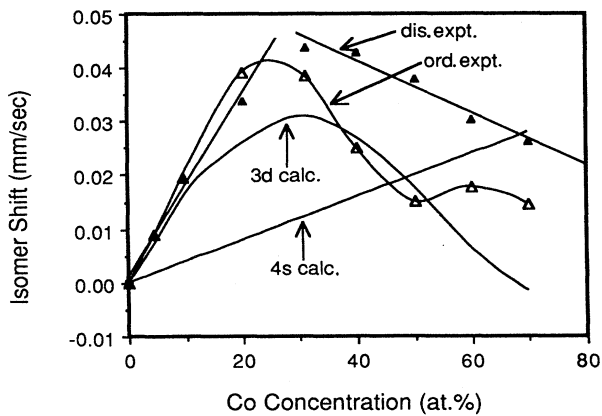


FIG. 5. The average ⁵⁷Fe isomer shift (relative to pure Fe) at 77 K vs Co concentration. The solid lines are least-squares fit to the experimental data. Also shown are the contributions of the Fe 3d and 4s electrons to the isomer shift of the disordered phase as obtained in Sec. III.

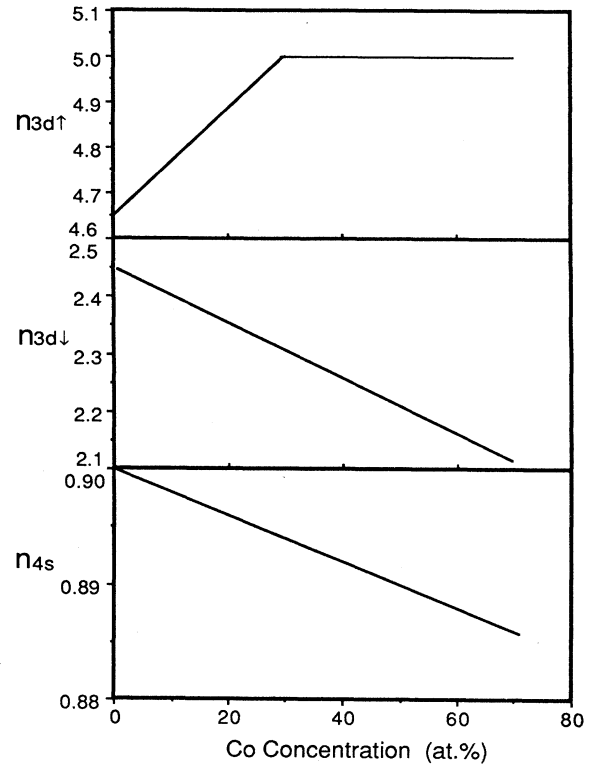


FIG. 6. The average number of electrons per atom in Fe 3d↑, 3d↓, and 4s states vs Co concentration for disordered Fe-Co alloys.

our isomer shift data; such large changes of up to 0.3 4s electrons would dominate the ⁵⁷Fe isomer shift.

We used the Mössbauer spectrometry results reported above to prepare Fig. 6, which shows the Co concentration dependence of the number of 4s electrons, together with the corresponding changes in the numbers of 3d↑ states and 3d↓ electrons at Fe atoms. The sum of the numbers of 3d↑ and 3d↓ electrons at Fe atoms is presented as a second curve in Fig. 4. In preparing Fig. 6, we used the estimate²⁶ for pure Fe that the number of 3d↑ electrons is about 4.65, while the number of 3d↓ electrons is about 2.45, and the number of 4s electrons is about 0.9. We emphasize that the main results of Fig. 6 were obtained using only data on magnetization and isomer shift. These electronic structure changes of Fe-Co alloys are essential to understanding the dependence of the ⁵⁷Fe HMF on Co concentration, as discussed next.

IV. HYPERFINE-MAGNETIC-FIELD DISTRIBUTION: ANALYSIS

Our analysis of hyperfine magnetic fields in disordered Fe-Co alloys follows that of Fultz and Morris for Fe-Ni alloys,²⁷ which is based on earlier work by Stearns,^{12,13} and Vincze and Campbell.^{4,28} The HMF at the ⁵⁷Fe nucleus is treated as two components. The first component is H_L , and is produced by the 3d electrons local to the ⁵⁷Fe atom through exchange polarizations of all s-like

electrons. This includes the core polarization (CP) of the 1s, 2s, and 3s electrons, as well as the conduction-electron polarization (CEP) of the 4s electrons. Changes in H_L are proportional to changes in the local magnetic moment at the ^{57}Fe atom, $\Delta\mu(0)$, induced by neighboring solute atoms:

$$\Delta H_L = (\alpha_{\text{CP}} + \alpha_{\text{CEP}}) \Delta\mu(0), \quad (3)$$

$$\Delta H_L = -86 \left[\frac{kG}{\mu_B} \right] \Delta\mu(0), \quad (4)$$

where α_{CP} and α_{CEP} are constants of proportionality between ΔH_L and $\Delta\mu(0)$ through the CP and CEP effects, respectively. We reference ΔH_L to the HMF of pure Fe metal. The second component is a transferred HMF, H_{NL} (nonlocal). It arises from spin polarizations (of 4s electrons at the ^{57}Fe nucleus) that are induced by exchange interactions with spins at neighboring atoms. For solute atoms at \mathbf{r} having magnetic moments, $\mu(\mathbf{r})$, differing from that of an Fe atom in pure Fe, μ_{Fe}^0 , the change in H_{NL} with respect to that in pure Fe is

$$\Delta H_{\text{NL}} = \alpha_{\text{CEP}} \sum_{\mathbf{r}(\neq 0)} f(\mathbf{r}) [\mu(\mathbf{r}) - \mu_{\text{Fe}}^0], \quad (5)$$

where $f(\mathbf{r})$ is the fraction of CEP at the Fe nucleus produced by a change in magnetic moment at \mathbf{r} , with respect to the CEP produced by the same change in magnetic moment at $\mathbf{r}=0$.

We separate ΔH_{NL} into two terms: ΔH_{DNL} and ΔH_{INL} . The term, ΔH_{DNL} (direct nonlocal), comprises the contributions from those lattice sites occupied by solute atoms. The term, ΔH_{INL} (indirect nonlocal), comprises the contributions from those lattice sites occupied by Fe atoms, but whose magnetic moments are perturbed by nearby Co atoms:

$$\Delta H_{\text{NL}} = \Delta H_{\text{DNL}} + \Delta H_{\text{INL}}, \quad (6)$$

$$\begin{aligned} \Delta H_{\text{DNL}} = & \alpha_{\text{CEP}} \sum_{\mathbf{r}(\neq 0)} \delta(\mathbf{r}) f(\mathbf{r}) \\ & \times \left[\left[\mu_X^0 + \sum_{\mathbf{r}' \neq \mathbf{r}} \delta(\mathbf{r}') g_X^X(|\mathbf{r}' - \mathbf{r}|) \right] \right. \\ & \left. - \mu_{\text{Fe}}^0 \right], \quad (7) \end{aligned}$$

$$\begin{aligned} \Delta H_{\text{INL}} = & \alpha_{\text{CEP}} \sum_{\mathbf{r}(\neq 0)} [1 - \delta(\mathbf{r})] f(\mathbf{r}) \\ & \times \sum_{\mathbf{r}' \neq \mathbf{r}} \delta(\mathbf{r}') g_X^{\text{Fe}}(|\mathbf{r}' - \mathbf{r}|). \quad (8) \end{aligned}$$

The Kronecker δ function equals 1 if the site is occupied by a solute atom, and equals 0 if it is occupied by an Fe atom. The variable $g_X^X(r)$ is the change in magnetic moment of a Y atom when it has an X solute in its r th coordination sphere. All perturbations of Fe magnetic moments are referenced to μ_{Fe}^0 , and all perturbations of solute magnetic moments are referenced to the magnetic moment of an isolated solute atom in a Fe matrix, μ_X^0 .

Using the same $\alpha_{\text{CEP}} f(\mathbf{r})$ parameters in both Eqs. (7) and (8) implicitly assumes the same amount of CEP per magnetic moment of either an Fe atom or a solute atom.

This assumption was found to be nearly true for Fe-Ni alloys,²⁷ and is expected to be a better approximation for Fe-Co alloys. For the set $\{\alpha_{\text{CEP}} f(1), \alpha_{\text{CEP}} f(2), \alpha_{\text{CEP}} f(3)\}$, we used $\{-11.5, -3.5, +2.5\}$ kG/ μ_B , as given by Fultz and Morris.²⁷ Because Al and Si solutes act as magnetic holes that only slightly perturb Fe or Co magnetic moments, the set of $\{\alpha_{\text{CEP}} f(\mathbf{r})\}$ parameters was checked for a Fe-50 at. % Co matrix by simulating the experimental Mössbauer spectra from Fe-49 at. % Co-2 at. % Al, Fe-48 at. % Co-4 at. % Al, and Fe-49 at. % Co-2 at. % Si alloys in terms of a main HMF distribution due to ^{57}Fe atoms without Al and Si neighbors, plus a satellite HMF distribution due to Fe atoms with Al and Si atom neighbors. The above set of $\alpha_{\text{CEP}} f(\mathbf{r})$ parameters gave a good fit to the experimental spectra.

Since the magnetic moment at Co atoms remains constant in Fe-Co alloys,^{4,20,21} the set $\{g_{\text{Co}}^{\text{Co}}(\mathbf{r})\} = \{0\}$. We used the set of $\{g_{\text{Co}}^{\text{Fe}}(\mathbf{r})\}$ parameters obtained from an NMR study of dilute Fe-Co alloys by Stearns,¹² although we scaled these parameters so that the calculated magnetization data were consistent with the experimental magnetization data of Bardos¹⁷ at low Co concentrations. At Co concentrations greater than about 10%, however, a saturation of the Fe magnetic moment produces Fe magnetic moments that are excessively enhanced by the second sum of Eq. (8) and produces simulated alloy magnetizations that exceed the experimental magnetizations. In order to match the magnetization data as well as possible, we employed a procedure whereby the Fe magnetic moment was smoothly saturated to $3.0\mu_B$.

In order to obtain the ^{57}Fe HMF distribution, a knowledge of the locations of all solute atoms in the alloy structure is required. This is best achieved by computer simulation. To simulate the rapidly quenched, disordered alloy, all sites of a bcc lattice were filled at random with either an Fe atom or a Co atom, according to the Co concentration. The simulations used the scaled $g_{\text{Co}}^{\text{Fe}}(\mathbf{r})$ parameters of Stearns¹² out to the fifth neighbor shell, and as mentioned above the primary sum in Eqs. (7) and (8) extended over the first three nearest-neighbor shells of each ^{57}Fe atom. The contributions: ΔH_L , ΔH_{DNL} , and ΔH_{INL} were evaluated at each Fe site, and the HMF distribution was obtained from the HMF's at all Fe sites. The average magnetization was obtained by summing the magnetic moments of all atoms in the alloy.

V. HYPERFINE-MAGNETIC-FIELD DISTRIBUTION: RESULTS AND DISCUSSION

The mean of the ^{57}Fe HMF distribution at 77 K versus Co concentration for both experiment and simulation are presented in Fig. 7. The simulated mean HMF exceeds that of the experimental data, especially at high Co concentrations. An analogous discrepancy was reported by Vincze, Campbell, and Meyer⁵ for their 295 K data, which were in excellent agreement with our own 295 K data. The difference in HMF between the simulated and experimental data at 77 K versus Co concentration is presented in Fig. 8. This discrepancy seems too large to be attributable to any difference in short range order be-

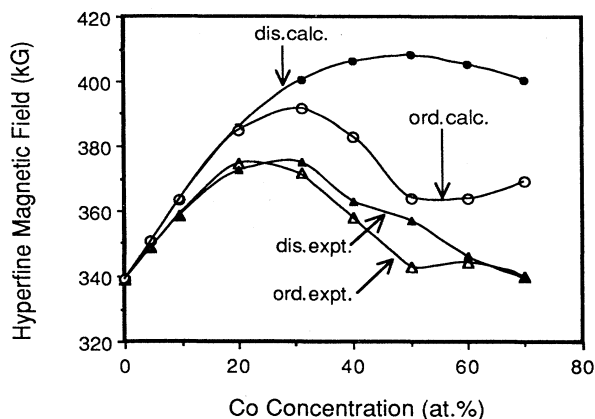


FIG. 7. The average ^{57}Fe HMF for disordered and ordered alloys at 77 K vs Co concentration. The calculated curves were obtained from the simulations described in Sec. IV.

tween the simulated and real alloys, and furthermore we would expect such a difference to have a maximum near 50 at. % Co, instead of being roughly linear with Co concentration. We can, however, readily attribute this difference between simulated and experimental data to the loss of $4s$ electrons found from the isomer shift data. The fact that the measured HMF is less negative than the simulated HMF indicates that it is mainly the $4s\downarrow$ state occupancy that decreases with Co concentration. The $4s$ hyperfine coupling constants from band calculations^{29,30} suggest that almost all the change in the $4s$ occupancy upon alloying is due to a loss of $4s\downarrow$ electron, whereas the smaller free ion coupling constants^{31,32} suggests that a modest increase in $4s\uparrow$ occupancies occurs as well. Perhaps as the Fe $3d\downarrow$ states form antibonding states and are repulsed to higher energy during alloying,¹⁹ they pull the Fe $4s\downarrow$ states with them by exchange interactions. A smaller, complementary process may occur with the $4s\uparrow$ states.

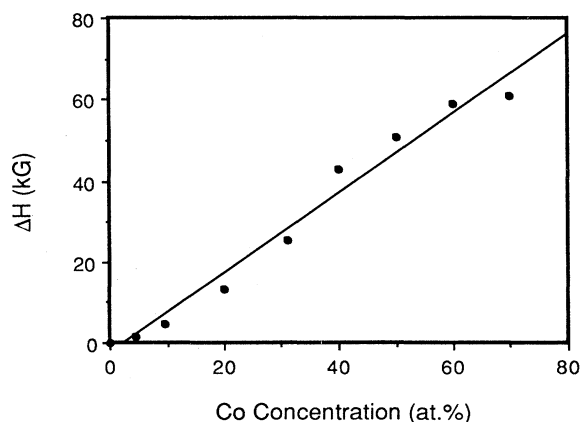


FIG. 8. The difference between experimental and simulated values of the mean ^{57}Fe HMF of disordered Fe-Co alloys at 77 K vs Co concentration. The solid line is least-squares fit to the experimental data.

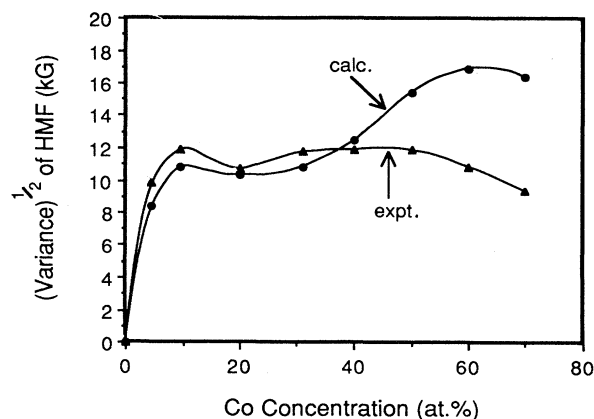


FIG. 9. The square root of the variance of the ^{57}Fe HMF distribution, $(\langle H^2 \rangle - \langle H \rangle^2)^{1/2}$, of disordered alloys at 77 K vs Co concentration.

Figure 9 presents the measured variances of the ^{57}Fe HMF distribution in Fe-Co alloys, together with the variances calculated by allowing no changes in $4s$ state occupancies. The overall agreement between the calculated and measured variances seems good, but we point out that the measured variance of the experimental HMF distribution for pure Fe was not zero, but had a square root of 4–5 kG. This implies that the calculated width of the HMF distribution is too large. The width of the HMF distribution reflects the inhomogeneity in local environments of ^{57}Fe nuclei. It seems that there is only a slight tendency of the delocalized $4s$ electrons to average over these local inhomogeneities, and the change in the number of $4s\downarrow$ electrons with Co concentration causes a discrepancy nearly as proportionally large as that of Fig. 8 for the mean HMF.

Some previous analyses of the shapes of HMF distributions in Fe-Co alloys have employed the assumption of Wertheim *et al.*¹¹ that the HMF perturbations of solutes in the various nearest-neighbor shells of the ^{57}Fe nucleus are additive. Additive perturbation parameters, such as those provided by Stearns,¹² can be used for very dilute Fe-Co alloys. These parameters, however, are not constant with Co concentration, primarily because of the dependence of ΔH_L and ΔH_{INL} on the magnetic moment of Fe atoms, and the saturation of the Fe magnetic moment with Co concentration. We found that the parameter " ΔH_1 ," for example, decreases with Co concentration and changes sign at a Co concentration around 50%. Even for dilute alloys, however, the use of additive perturbation parameters must be done cautiously, and must include parameters up to the fifth nearest-neighbor shell.

"Anisotropic" or "pseudodipolar" HMF perturbations were first found in the single crystal experiments of Cranshaw *et al.*³³ With our polycrystalline materials we made a rough measurement of the strength of the anisotropic contributions to the ^{57}Fe HMF in the Fe–50 at. % Co alloy. By applying a uniform 2 kG magnetic field perpendicularly to the incident γ -ray direction, we oriented the magnetization directions randomly with respect to

the crystalline axes of the grains of the alloy. We measured a broadening of the HMF distribution of 1–2 kG with respect to that obtained without an applied magnetic field. Assuming that the magnetization direction relaxes to a $\langle 100 \rangle$ easy axis without any applied field, we deduce that the anisotropic component of the HMF perturbations is due to $1nn$ atoms and is rather weak, having a magnitude approximately comparable to that of Fe-Ni.^{27,34}

We explored the sensitivity of our simulated HMF distributions to variations in the s -electron polarization parameters. Ten percent variations of both the sum ($\alpha_{CP} + \alpha_{CEP}$), and the set of conduction electron polarizations by Co atoms $\{\alpha_{CEP}f(r)\}$, affected the average HMF by less than 5 kG and 1 kG, respectively, at any Co concentration. Other sets of $\{\alpha_{CEP}f(r)\}$ were used: $\{-12.1, -2.7, +2.4\}$ (kG/ μ_B),¹² and $\{-11.0, -0.9, -2.4\}$ (kG/ μ_B).³⁵ With the former set we obtain results essentially identical to those of Sec. IV, and the latter set provided an average HMF that was higher by no more than 7 kG. None of these results would alter our conclusion that the simulated HMF distributions imply a reduced occupancy of $4s \downarrow$ states with increasing Co concentration. Some previous workers have used a smaller value for the Co magnetic moment, $1.6\mu_B$ for example.^{4,22} Using a lower value for the Co magnetic moment would serve to increase both the difference between the numbers of $3d \uparrow$ and $3d \downarrow$ electrons in Fig. 6 and the discrepancy in Fig. 8, and would require a greater imbalance of $4s \uparrow$ and $4s \downarrow$ electrons with increasing Co concentration. Our results of Fig. 6 would remain qualitatively the same at low Co concentrations, however, changing by about 25%. Finally, we note that the changes in $4s$ state occupancy of Fig. 6 are quite small, and in a free electron gas they do not alter the value of the Fermi wave vector enough to significantly influence the CEP parameters: $\{\alpha_{CEP}f(r)\}$.

VI. ORDERED Fe-Co ALLOYS

The isomer shift, magnetization, and HMF undergo changes as a result of $B2$ chemical ordering. It appears that the change in isomer shift after ordering is different for alloy compositions below and above about 30 at. % Co (see Fig. 5).^{36,37} In alloys with less than about 30 at. % Co, the addition of more Co atoms to the first nearest-neighbor shell of ^{57}Fe atoms upon $B2$ ordering increases the total number of electrons in the $3d \uparrow$ states of the ^{57}Fe atom, which causes the isomer shift to increase. In alloys with more than 30 at. % Co the Fe $3d \uparrow$ states are full, and the addition of Co atoms to the neighborhoods of ^{57}Fe atoms will only decrease the number of electrons in the $3d \downarrow$ states, which causes the isomer shift to decrease. It seems that a loss of 0.12 $3d \downarrow$ electrons could account for the observed change in magnetic moment (Fig. 3) and isomer shift (Fig. 5) during ordering. From Fig. 7 we see that the calculated change in mean HMF upon ordering exceeds considerably that of experiment. We do not believe that this discrepancy arises from an overestimate of changes in $3d$ spin polarizations

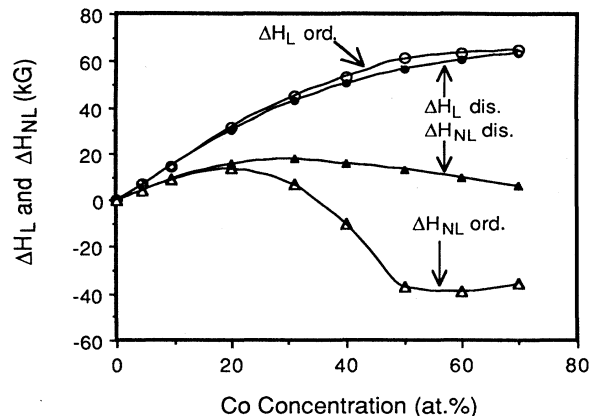


FIG. 10. Calculated local and nonlocal components of the ^{57}Fe HMF (H_L and H_{NL}), vs Co concentration. (These results are not corrected for changes in the $4s$ polarization with alloying.)

during ordering; as seen in Fig. 3 the calculated change in magnetic moment agrees fairly well with that of experiment, even underestimating the experimental trend at Fe–50 at. % Co. Instead we believe that there is a change in the spin polarization of the $4s$ electrons during ordering. If we assume that the change in isomer shift can be mostly accounted for by the loss of $3d \downarrow$ electrons during ordering, it then appears that this discrepancy is due to a simultaneous increase in $4s \downarrow$ electrons and decrease in $4s \uparrow$ electrons during ordering.

The magnetic moment of Fe atoms is larger in ordered than in disordered alloys (see Fig. 3), since in the ordered structure Fe atoms have more Co atoms as first nearest neighbors. Although the magnetic moment of Fe atoms increases upon ordering, the magnitude of the HMF decreases (see Fig. 7). At 50 at. % Co, $H_{\text{order}} - H_{\text{disorder}} = +8$ kG at 295 K, and increases to +14.5 kG at 77 K. Very similar values for $H_{\text{order}} - H_{\text{disorder}}$ at 295 K have been reported by others,^{5,6} in spite of the differences in producing the disordered alloys. An understanding of why the magnitude of the HMF decreases upon ordering, whereas the magnetization increases, requires consideration of all contributions to the ^{57}Fe HMF. The individual contributions to the ^{57}Fe HMF, ΔH_L , ΔH_{DNL} , and ΔH_{INL} were obtained from simulated ordered and disordered alloys,^{38,39} and the change in the local and nonlocal components of the average ^{57}Fe HMF upon ordering are presented in Fig. 10. It is clear that the nonlocal contribution to the ^{57}Fe HMF undergoes the greatest change upon ordering, and most of this is due to changes in ΔH_{INL} , although changes in ΔH_{DNL} are also significant. This points out an important aspect of using Mössbauer spectrometry to measure chemical order in Fe-Co alloys: The spatial range over which Mössbauer spectra are sensitive to local atomic arrangements is the longer characteristic length of the Fe-magnetic-moment perturbations around Co atoms, not the shorter characteristic length of the conduction-electron polarizations. Nevertheless, our preliminary results indicate that while many previous Mössbauer spectrometry investigations of the order-

disorder transformation in Fe-Co have improperly attributed the ^{57}Fe HMF to additive HMF perturbations, the resulting relationships between average HMF and short range order parameter are strikingly similar to our own.⁴⁰ We are presently studying in greater detail the dependence of Mössbauer spectra of Fe-Co alloys on the local atomic order. It seems that ^{57}Fe atoms associated with two types of defects in the ordered structure, ^{57}Fe atoms near antiphase domain boundaries and ^{57}Fe atoms situated of Co sites, have large HMF's and result in a positive skewness of the HMF distribution in partially ordered alloys. A bit of this positive skewness is evident in Fig. 2 in the HMF distribution from the mostly ordered alloy.

VII. CONCLUSION

We have performed Mössbauer spectrometry measurements of the HMF distribution and average isomer shift in bcc Fe-Co alloys, along with some EELS measurements of 3d-state occupancies. Together with bulk magnetization data, we deduce how the occupancies of the 3d \uparrow and 3d \downarrow states at Fe atoms change with Co concentration, consistent with the assumption of a transition from weak to strong ferromagnetism at around 30 at. % Co. Charge transfers involving 3d electrons to the Fe 3d states (at 30 at. % Co) were found to be no greater than +0.2 by Mössbauer spectrometry and magnetization data, and about -0.3 electrons by EELS. Both our iso-

mer shift and HMF data indicate a slight reduction in the occupancy of 4s states with Co concentration of $dn_{4s}/dc = -0.02$ electrons, principally due to a loss of 4s \downarrow electrons.

The model employed for the calculation of HMF distributions, which includes responses of both the core electron polarizations and the conduction electron polarizations to magnetic moments, was found to work well for disordered Fe-Co alloys. Although the HMF perturbations of Co atoms in the various nearest-neighbor shells of ^{57}Fe atoms are additive at dilute Co concentrations, these additive HMF perturbation parameters become strongly concentration dependent, even changing sign, at higher concentrations. The model was also used to analyze the changes in mean HMF after the disorder \rightarrow order transformation and showed that these changes originate mostly from the CEP response to changes in the Fe magnetic moments after ordering. This implies that Mössbauer spectra are sensitive to atomic arrangements over distances up to 9 Å around the ^{57}Fe atoms.

ACKNOWLEDGMENTS

The authors thank C. C. Ahn for help with the EELS measurements. This work was supported by the U.S. Department of Energy under Contract No. DE-FG03-86ER45270.

- ¹A. R. Williams, V. L. Moruzzi, A. P. Malozemoff, and K. Terakura, IEEE Trans. Magn. **MAG-19**, 1983 (1983).
- ²R. H. Victora and L. M. Falicov, Phys. Rev. **B 30**, 3896 (1984).
- ³E. C. Sowa and L. M. Falicov, Phys. Rev. **B 37**, 8707 (1988).
- ⁴R. Richter and H. Eschrig, J. Phys. **F 18**, 1813 (1988).
- ⁵I. Vincze, I. A. Campbell, and A. J. Meyer, Solid State Commun. **15**, 1495 (1974).
- ⁶J. P. Eymery, S. B. Raju, and P. Moine, Phys. Lett. **68A**, 260 (1978).
- ⁷G. K. Wertheim, Phys. Rev. **B 1**, 1263 (1970).
- ⁸A. Narayanasamy *et al.*, J. Phys. **F 9**, 2261 (1979).
- ⁹B. deMayo, Phys. Rev. **B 24**, 6503 (1981).
- ¹⁰J. E. Frackowiak, Phys. Status Solidi **87**, 109 (1985).
- ¹¹G. K. Wertheim, V. Jaccarino, J. H. Wernick, and D. N. E. Buchanan, Phys. Rev. Lett. **12**, 24 (1964).
- ¹²M. B. Stearns, Phys. Rev. **B 9**, 2311 (1974).
- ¹³M. B. Stearns, Phys. Rev. **B 13**, 1183 (1976).
- ¹⁴J. I. Budnick, T. J. Burch, S. Skalski, and K. Raj, Phys. Rev. Lett. **24**, 511 (1970).
- ¹⁵D. H. Pearson, B. Fultz, and C. C. Ahn, Appl. Phys. Lett. **53**, 1405 (1988).
- ¹⁶G. Le Cäer and J. M. Dubois, J. Phys. **E 12**, 1083 (1979).
- ¹⁷D. I. Bardos, J. Appl. Phys. **40**, 1371 (1969).
- ¹⁸P. Weiss and R. Forrer, Ann. Phys. **12**, 279 (1929).
- ¹⁹H. Hasegawa and J. Kanamori, J. Phys. Soc. Jpn. **33**, 1607 (1972).
- ²⁰N. Hamada, J. Phys. Soc. Jpn. **46**, 1759 (1979).
- ²¹M. F. Collins and J. B. Forsyth, Philos. Mag. **8**, 401 (1963).
- ²²K. Schwarz, P. Mohn, P. Blaha, and J. Kubler, J. Phys. **F 14**, 2659 (1984).
- ²³S. Suzuszkiewicz, Phys. Status Solidi **140**, 141 (1987).
- ²⁴L. R. Walker, G. K. Wertheim, and V. Jaccarino, Phys. Rev. Lett. **6**, 98 (1961).
- ²⁵G. A. Fateseas, Phys. Rev. **B 8**, 43 (1973).
- ²⁶S. Wakoh and J. Yamashita, J. Phys. Soc. Jpn. **21**, 1712 (1966).
- ²⁷B. Fultz and J. W. Morris, Jr., Phys. Rev. **B 34**, 4480 (1986).
- ²⁸I. Vincze and I. A. Campbell, J. Phys. **F 3**, 647 (1973).
- ²⁹K. J. Duff and T. P. Das, Phys. Rev. **B 3**, 192 (1971).
- ³⁰S. Wakoh and J. Yamashita, J. Phys. Soc. Jpn. **25**, 1272 (1968).
- ³¹R. E. Watson and A. J. Freeman, Phys. Rev. **123**, 2027 (1961).
- ³²R. E. Watson and L. H. Bennett, Phys. Rev. **B 15**, 502 (1977).
- ³³T. E. Cranshaw, C. E. Johnson, M. S. Ridout, and G. A. Murray, Phys. Lett. **21**, 481 (1966).
- ³⁴T. E. Cranshaw, in *Industrial Applications of the Mössbauer Effect*, edited by G. Long and J. G. Stevens (Plenum, New York, 1986), p. 7.
- ³⁵I. Vincze and L. Cser, Phys. Status Solidi **B 50**, 709 (1972).
- ³⁶Although the order-disorder transformation at our Co concentration of 20 at. % Co would be at a temperature out of the range of the recently assessed Co-Fe phase diagram (Ref. 37), we expect short-range order to evolve during annealing.
- ³⁷T. Nishizawa and K. Ishida, Met. Prog. **125**, 57 (1986).
- ³⁸Disordered and ordered alloys of equiatomic compositions were easily obtained. Ordered alloys with Co concentrations other than 50% were generated by a Monte Carlo algorithm (Ref. 39) that simulated the process of ordering on a bcc lattice by a vacancy mechanism. At a suitably low temperature, the algorithm was run until the long and short range order parameters of the alloy no longer changed, and the HMF distribution was then evaluated.
- ³⁹B. Fultz, J. Chem. Phys. **87**, 1604 (1987).
- ⁴⁰B. Fultz, H. H. Hamdeh, and D. H. Pearson (unpublished).